Baryon-antibaryon pair production in time-dependent meson fields

I. N. Mishustin,[1,2] L. M. Satarov,[1] H. Stöcker,[3] and W. Greiner[3]

[1]The Kurchatov Institute, Moscow 123182, Russia

[2]The Niels Bohr Institute, Blegdamsvey 17, DK–2100, Copenhagen Ø, Denmark

[3]Institut für Theoretische Physik, J.W. Goethe Universität, D-60054 Frankfurt am Main, Germany

Strong mean meson fields, which are known to exist in normal nuclei, experience a violent deformation in the course of a heavy-ion collision at relativistic energies. This may give rise to a new collective mechanism of the particle production, not reducible to the superposition of elementary nucleon-nucleon collisions. We study the baryon-antibaryon ($N\bar{N}, \Lambda\bar{\Lambda}, \ldots$) pair production under some simplifying assumptions about the space and time variation of meson fields in the nuclear collision process. The mutual deceleration of nuclei is described schematically by introducing the time-dependent relative velocity. For comparison the yield of $N\bar{N}$ pairs is also calculated within a convolution model assuming the same deceleration scenario. Due to the specific Lorentz structure, the vector meson field turns out to be more efficient for producing pairs than the scalar field. Within the perturbative approach we study two processes: the bremsstrahlung of a virtual meson and the fusion of two virtual mesons, both leading to the baryon-antibaryon final states. The calculated multiplicities of $N\bar{N}$ and $\Lambda\bar{\Lambda}$ pairs grow fast with the bombarding energy, reaching a saturation above the RHIC energy ($\sqrt{s} = 200A$ GeV). At lower energies the coherent production mechanism gives higher pair yields than predicted by microscopic cascade-like models. The rapidity spectra of antibaryons exhibit a characteristic two-hump structure which may serve as an observable signature of the bremsstrahlung mechanism. A strong sensitivity of the predicted yield to the baryon effective mass and the parameters characterizing the stopping power of nuclear matter is demonstrated.

I. INTRODUCTION

In relativistic heavy-ion collisions the hadronic matter is produced in states which are very far from the nuclear ground state. If thermal equilibrium is established at some stages of the collision process, one can characterize the matter by the equation of state. Despite much efforts made to extract the information about the equation of state, the conclusions still remain uncertain, especially at high bombarding energies. One cannot even say what degrees of freedom, hadrons or quarks and gluons, are more suitable for describing these collisions. Fast dynamics, relativistic effects in particle interactions, and a finite formation time for hadrons make the picture less trivial but not necessarily more complicated. At ultrarelativistic energies, due to the limited stopping power of nuclear matter, the two colliding nuclei do not stop in the center-of-mass frame, but rather interpenetrate through each other losing a fraction of the initial kinetic energy for producing new particles and exciting the matter [1].

In this paper we consider a purely dynamical, collective mechanism of particle production based on the relativistic picture of a nucleus as composed of nucleons interacting with meson fields. According to the relativistic mean-field model [2], strong scalar and vector mean fields are generated in the nuclear interior. In some aspects the collision of relativistic nuclei can be viewed as the interaction of these meson fields, Lorentz boosted to a proper reference frame. In the course of interpenetration two bumps of meson fields are slowing down and acquire deformation. Moreover, they can be partially or totally destroyed if the coherence does not persist at the violent stage of the reaction. In any case, one is

dealing here with time-dependent "external" fields which can produce particles via the Schwinger mechanism [3]. Below we show that in some cases this coherent mechanism of particle production may be more efficient than the incoherent superposition of nucleon-nucleon collisions.

As shown in Refs. [4,5] strong meson fields generated in relativistic nuclear collisions may also give rise to the "spontaneous" baryon-antibaryon pair production, through the decay of "negative" energy Dirac sea inside the compressed nuclear matter. To study the observable signals of this phenomenon one should also know the contribution of the induced processes associated with high Fourier frequencies of meson fields generated in the course of a nuclear collision. A strong enhancement of antibaryon yields associated with the reduction of their effective mass in thermally equilibrated system was demonstrated in Ref. [6].

Unfortunately, the space-time structure of meson fields is rather complicated and there is no hope to find the exact solution of the particle production problem. Therefore, our calculations will be performed mostly within the perturbative approach. In many respects the formalism is similar to that used for the particle production by electromagnetic fields induced in relativistic heavy-ion collisions [7–12]. Two collective processes are considered below: the bremsstrahlung of virtual mesons with their subsequent decay into the baryon-antibaryon ($B\bar{B}$) pairs and the pair production by the collision (fusion) of two virtual ω-mesons. In the latter case, in close analogy to the equivalent photon picture [13] for the Lorentz-boosted Coulomb field, one can represent mean meson fields in a fast moving frame as beams of virtual mesons characterized by certain spatial and spectral distributions. Then the cross section of any process induced by time-

dependent "classical" fields may be expressed through the cross section of the elementary process involving two virtual quanta of these fields.

We would like to note that the collective mechanism of pion production by nuclear fields generated in heavy-ion collisions ("pion bremsstrahlung") was studied earlier in Refs. [14,15]. The dynamics of the meson fields in the course of a nuclear collision was considered in Refs. [16–19] by the direct solving the time-dependent Dirac equation. The classical radiation of real ω mesons caused by transverse fluctuations of the vector field in nuclear collisions was considered in Ref. [20].

In this paper we focus mainly on the $B\overline{B}$ pair production by strong meson fields associated with relativistic nuclear collisions. In Sec. II the general formalism is presented. In Secs. III and IV it is applied for calculating the $B\overline{B}$ pair production by the bremsstrahlung and meson-meson fusion. The incoherent (direct) production of pairs in binary nucleon-nucleon collisions is considered in Sec. V. The numerical results are given in Sec. VI. The discussion and conclusions are presented in Sec. VII.

II. GENERAL FORMALISM

The probability $W_{i_+i_-}$ to produce a baryon(B)-antibaryon($\overline{B}$) pair in the quantum state $i_+(B)i_-(\overline{B})$ can be written as

$$W_{i_+i_-}=|M_{i_+i_-}|^2.\qquad(1)$$

Here $i_\pm=p_\pm,\sigma_\pm,\tau_\pm$ denote briefly the momenta ($p_\pm$), spins ($\sigma_\pm$), and isospins ($\tau_\pm$) of the particles, $M_{i_+i_-}$ is the transition amplitude of the process: "external" meson field $\rightarrow B_{i_+}\overline{B}_{i_-}+X$. It can be expressed in terms of the S matrix

$$M_{i_+i_-}=\langle 0|a_{i_+}b_{i_-}S|0\rangle,\qquad(2)$$

where $|0\rangle$ is the "vacuum" state containing external meson fields and no pairs, $a_{i_+}(b_{i_-})$ is the annihilation operator for a baryon (antibaryon) in the state $i_+(i_-)$.

Quite generally one can write[1]

$$S=T\exp\left\{i\int d^4x\mathcal{L}_{\rm int}(x)\right\}$$
$$=1+S^{(1)}+S^{(2)}+\cdots,\qquad(3)$$

where $S^{(1)},S^{(2)},\ldots$, are the contributions of the first, second, ..., order in the external field. Denoting by $\mathcal{A}(x)$ the amplitude of this field in a space-time point x one can represent the interaction Lagrangian density as

$$\mathcal{L}_{\rm int}=:\overline{\Psi}_B(x)\mathcal{A}(x)\Psi_B(x):,\qquad(4)$$

where the notation $:\cdots:$ is used for the normal product of operators. The baryon field operator $\Psi_B(x)$ is represented in a standard second quantization form [21]

$$\Psi_B(x)=\sum_i[a_i\Psi^{(+)}(x)+b_i^+\Psi^{(-)}(x)].\qquad(5)$$

As before, $a_i(b_i)$ and $a_i^+(b_i^+)$ denote the annihilation and creation operators of a baryon (antibaryon) in the state i. They obey the fermion anticommutation relations

$$\{a_i,b_j\}=0,\quad\{a_i,a_j^+\}=\{b_i,b_j^+\}=\delta_{ij}.\qquad(6)$$

The general Lorentz structure of the external field associated with nuclear mean meson fields can be expressed as

$$\mathcal{A}(x)=S(x)-\gamma_\mu V^\mu(x),\qquad(7)$$

where $S(x)$ and $V_\mu(x)$ are, respectively, the scalar and four-vector parts of the fields. In the mean-field approximation they are treated as c numbers:

$$S(x)=g_S\sigma(x),\quad V^\mu(x)=g_V\omega^\mu(x),\qquad(8)$$

where $\sigma(x)$ and $\omega_\mu(x)$ are the usual nuclear σ and ω fields coupled to nucleons with coupling constants g_S and g_V. These fields are determined self-consistently by the nuclear sources:

$$(\Box+m_\sigma^2)\sigma(x)=g_S\rho_S(x),\qquad(9)$$

$$(\Box+m_\omega^2)\omega^\mu(x)=g_V J^\mu(x).\qquad(10)$$

Here $\Box\equiv\partial_t^2-\Delta$, the scalar density ρ_S and the four-current J_μ of nucleons are, respectively,

$$\rho_S(x)=\langle\overline{\Psi}_N(x)\Psi_N(x)\rangle,\qquad(11)$$

$$J^\mu(x)=\langle\overline{\Psi}_N(x)\gamma^\mu\Psi_N(x)\rangle.\qquad(12)$$

Averaging over the microscopic states of the system is implied in Eqs. (11) and (12).

At high energies when nuclei are partially transparent to each other, one can treat a heavy-ion collision as an interaction of two interpenetrating baryonic flows originating from the projectile and target nuclei. The four-current can be expressed as

$$J_\mu(x)=\sum_{\alpha=p,t}\rho_V^{(\alpha)}(x)U_\mu^{(\alpha)}(x),\qquad(13)$$

where $\rho_V^{(\alpha)}(x)$ and $U_\mu^{(\alpha)}(x)$ are, respectively, the rest-frame vector density and the four-velocity of the projectile ($\alpha=p$) and target ($\alpha=t$) flow. Due to the local conservation of the baryon current [$\partial_\mu J^\mu(x)=0$] the vector field satisfies an additional constraint

$$\partial_\mu V^\mu(x)=0.\qquad(14)$$

Below we use the momentum representation of the fields. The Fourier transformed meson field is defined as

$$\mathcal{A}(p)=\int d^4x e^{ipx}\mathcal{A}(x)=S(p)-\gamma_\mu V^\mu(p),\qquad(15)$$

---

[1]Units with $\hbar=c=1$ are used throughout the paper.

where $px = p^0 t - \mathbf{pr}$. The corresponding transformations are also introduced for $\rho_S(x)$ and $J^\mu(x)$. Using this representation one can solve Eqs. (9) and (10) (for $p^2 \neq m_\sigma^2, m_\omega^2$), and get

$$S(p) = -D_S(p)\rho_S(p), \tag{16}$$

$$V^\mu(p) = -D_V(p)J^\mu(p). \tag{17}$$

Here

$$D_S(p) = \frac{g_S^2}{p^2 - m_\sigma^2} f_S(p), \tag{18}$$

$$D_V(p) = \frac{g_V^2}{p^2 - m_\omega^2} f_V(p), \tag{19}$$

are the corresponding Green functions. Formally the solutions of Eqs. (9) and (10) correspond to $f_i = 1$ ($i = S, V$). By inserting additional form factors $f_i(p)$ we introduce the corrections to the SNN and VNN vertices due to the composite structure of nucleons.

We choose the monopole type parametrization of f_i

$$f_i(p) = \frac{\Lambda_i^2}{\Lambda_i^2 + p^2}, \tag{20}$$

where the cutoff masses $\Lambda_i \sim 2$ GeV [22]. These intrinsic form factors of nucleons suppress the emission of mesons at large p^2. The experimental information concerning the form factors $f_i(p)$ is rather controversial [23]. In particular, the characteristics of $f_V(p)$ may be indirectly extracted from the data on the electromagnetic nucleon form factors within the vector meson dominance model [24].

In the momentum representation the condition (14) has the form

$$[p \cdot V(p)] = 0. \tag{21}$$

According to Eqs. (13) and (17) the vector field is the sum of the projectile and target vector fields. This is not the case for the scalar field. Due to the nonlinear terms the latter is smaller [5] than the simple sum of the scalar fields from the projectile and target nuclei in the region of their geometric overlap.

Below the explicit formulas are given for the case of the $N\bar{N}$ pairs. The analogous expressions for other (e.g., $\Lambda\bar{\Lambda}$) pairs can be obtained by replacing the corresponding baryon masses and coupling constants. We use the standard representation of the (anti)nucleon wave functions [21], introduced in Eq. (5):

$$\begin{Bmatrix} \Psi_i^{(+)} \\ \Psi_i^{(-)} \end{Bmatrix} = \sqrt{\frac{m_N}{E_i \Omega}} \begin{Bmatrix} u_i e^{-i p_i x} \\ v_i e^{+i p_i x} \end{Bmatrix}. \tag{22}$$

Here $p_i = (E_i, \mathbf{p}_i)$ is the four-momentum of the (anti)nucleon, $E_i = \sqrt{m_N^2 + \mathbf{p}_i^2}$ is its energy, m_N and Ω are, respectively, the nucleon mass and the normalization volume. The bispinors u_i, v_i are normalized according to the relation
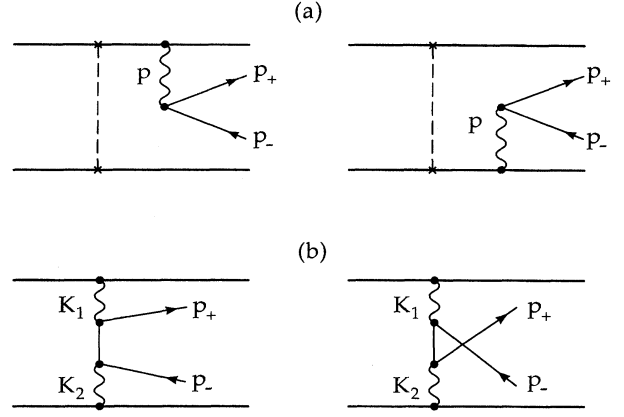

FIG. 1. Lowest order Feynman diagrams for the production of $N\bar{N}$ pair in nuclear collisions. Parts (a) and (b) correspond, respectively, to bremsstrahlung and second order (fusion) processes. Wavy lines denote mean-field interaction. Thin solid lines denote propagation of fermions. Upper and lower thick lines correspond to projectile and target nuclei, respectively. Dashed line shows an arbitrary interaction which causes mutual deceleration of nuclei.

$$\bar{u}_i u_i = -\bar{v}_i v_i = 1. \tag{23}$$

A straightforward calculation based on Eqs. (2)–(6) and (22) yields the following expressions for the pair-production amplitudes in the first two orders in $\mathcal{L}_{\text{int}}$:

$$M_{i_+ i_-}^{(1)} = -\frac{i m_N}{\Omega \sqrt{E_+ E_-}} \bar{u}_{i_+} \mathcal{A}(p_+ + p_-) v_{i_-}, \tag{24}$$

$$M_{i_+ i_-}^{(2)} = -\frac{i m_N}{\Omega \sqrt{E_+ E_-}} \bar{u}_{i_+} \int \frac{d^4 q}{(2\pi)^4} \mathcal{A}(p_+ - q) G(q)$$

$$\times \mathcal{A}(q + p_-) v_{i_-}, \tag{25}$$

where

$$G(q) = \frac{\hat{q} + m_N}{q^2 - m_N^2 + i\delta} \tag{26}$$

is the vacuum Green function of nucleons. The Feynman diagrams corresponding to the amplitudes (24) and (25) are shown in Figs. 1(a) and 1(b), respectively.

It is easy to see that the first order contribution (24) is nonzero only if $\mathcal{A}(p) \neq 0$ for $p^2 > 4m_N^2$. Since $V_\mu(p) \propto J_\mu(p)$ contain a large γ factor of the projectile-target relative motion, the relation

$$|V_\mu^*(p) V^\mu(p)| \gg |S(p)|^2 \tag{27}$$

usually holds at high bombarding energies. Let τ denote a characteristic time of the nuclear density variation in the rest frame of the corresponding nucleus. In the region $|p_0| \gg \tau^{-1}$ the vector field $V_\mu(p)$ is exponentially small and condition (27) may be violated. For example, in the free-streaming approximation ($\tau = \infty$) both nuclei interpenetrate without mutual deceleration. As will be shown in Sec. III, in this case $V_\mu(p) \neq 0$ only in the spacelike region $p^2 < 0$ and,
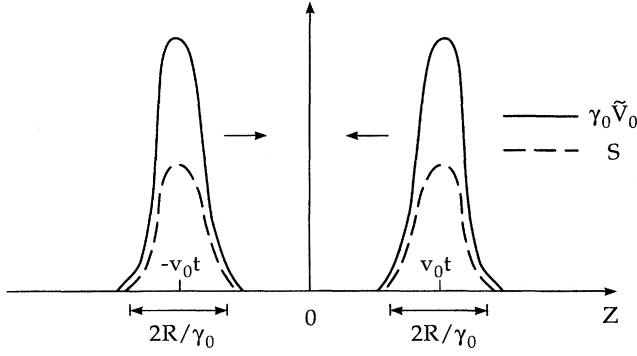
FIG. 2. Scalar (dashed line) and vector (solid line) meson potentials before a central collision of identical nuclei shown as a function of longitudinal coordinate z in the equal velocity frame (schematic view). Only time-like component of vector potential is shown ($\tilde{V}_0$ is the corresponding potential in the nucleus rest frame).

therefore, the first order contribution of the vector field vanishes. In this case the pair production is possible only in the second and higher order processes. In a more realistic scenario, the collisional and mean-field interaction of nuclei lead to their mutual deceleration. As a consequence, the $N\bar{N}$ pairs may be produced already in the first order process, since nonzero Fourier components of the meson field appear in the timelike region $p^2 > 4m_N^2$. By analogy to the e^+e^--pair production by an accelerating charged particle, we refer the first order processes [Fig. 2(a)] as the pair production due to the bremsstrahlung of the σ, ω mesons. This process is similar to the pion bremsstrahlung considered in Refs. [14,15].

The momentum distribution of pairs is proportional to the probability density (1)

$$\frac{d^6N}{d^3p_+ d^3p_-} = \frac{\Omega^2}{(2\pi)^6} \sum_{\sigma_\pm, \tau_\pm} W_{i_+ i_-}. \tag{28}$$

Equations (24) and (25) yield the following expression for the spectrum of the $N\bar{N}$ pairs:

$$E_+ E_- \frac{d^6N}{d^3p_+ d^3p_-} = \frac{d_\tau}{4(2\pi)^6} \mathrm{Sp}\{(\hat{p}_- - m_N)\overline{\mathscr{B}}(p_+, p_-)$$
$$\times (\hat{p}_+ + m_N)\mathscr{B}(p_+, p_-)\}, \tag{29}$$

where d_τ is the isospin degeneracy factor and

$$\mathscr{B}(p_+, p_-) = \mathscr{A}(p_+ + p_-) + \int \frac{d^4q}{(2\pi)^4} \mathscr{A}(p_+ - q)G(q)$$
$$\times \mathscr{A}(q + p_-). \tag{30}$$

Here the first term is associated with the bremsstrahlung process [Fig. 1(a)] and the second term describes the pair production by the fusion of meson fields.

Due to the charge conservation only the $p\bar{p}$ and $n\bar{n}$ pairs may be produced by the considered coherent mechanism. One should substitute $d_\tau = 1$ or $d_\tau = 2$ to obtain the yield of charged ($p\bar{p}$) or all ($p\bar{p} + n\bar{n}$) $N\bar{N}$ pairs.

Let us discuss briefly the geometrical picture of a heavy ion collision. As in Refs. [10,14], we assume that at the stage of the projectile-target interpenetration the two nuclei move as a whole along the beam axis with a mutual deceleration. We describe them as Lorentz-contracted ellipsoids whose widths are determined by the instantaneous γ factors. We also assume that they have the rest-frame densities of initial nuclei. Therefore, the compression and the transverse motion of nuclear matter are disregarded by the model.

Below we consider the central collisions of identical nuclei (at zero impact parameter). The calculations are performed in the equal velocity (e.v.) frame where the nuclei move with velocities $\dot{\xi}_p = -\dot{\xi}_t \equiv \dot{\xi}$ and have a Lorentz-factor $\gamma = (1 - \dot{\xi}^2)^{-1/2}$. Choosing the z axis along the beam direction one can parametrize the four-velocities and the densities of interpenetrating nuclei as follows ($\alpha = p, t$):

$$U_\mu^{(\alpha)}(x) = [\gamma(t), 0, 0, \mp \gamma(t)\dot{\xi}(t)]_\mu, \tag{31}$$

$$\rho_V^{(\alpha)}(x) = \rho_V[\sqrt{r_\perp^2 + \gamma^2(t)[z \mp \xi(t)]^2}]. \tag{32}$$

Here the upper (lower) sign corresponds to the projectile (target) nucleus, $r_\perp = (x, y)$ stands for spatial coordinates in the transverse directions. The function $\rho_V(r)$ in Eq. (32) is the rest-frame vector density of the initial nucleus. According to Eqs. (16) and (17) the meson fields are entirely determined by the scalar density and four-vector current of nucleons. A schematic picture of spatial distribution of meson fields at the initial stage of nuclear reaction ($\dot{\xi} \approx v_0$) is shown in Fig. 2.

Two parametrizations of $\rho_V(r)$ are considered. First one is the homogeneous sphere distribution

$$\rho_V(r) = \rho_0 \Theta(R - r), \tag{33}$$

where $\rho_0 = 0.17$ fm^{-3} is the normal nuclear density, R is the radius of initial nuclei, and $\Theta(x) \equiv (1 + \mathrm{sign}x)/2$. The corresponding density form factor in the momentum space is

$$F(q) \equiv \frac{1}{A} \int d^3r \rho_V(r)e^{-iqr} = \frac{3}{x^2}\left(\frac{\sin x}{x} - \cos x\right)\bigg|_{x=qR}. \tag{34}$$

Here $A = 4\pi\rho_0 R^3/3$ is the mass number of a nucleus.

The calculations show that the neglect of density smoothing at the nuclear boundary leads to a noticeable overestimation of the pair yield as compared to the more realistic Woods-Saxon distribution:

$$\rho_V(r) = \frac{\rho_1}{1 + \exp\left(\dfrac{r - R}{a}\right)}. \tag{35}$$

The normalization constant ρ_1 is determined from the condition $\int d^3r \rho_V = A$. In our calculation we choose $R = 1.12A^{-1/3}$ fm, $a = 0.5$ fm. The form factor corresponding to the distribution (35) may be written in a semianalytic form by using the representation of the Fermi-like integrals as a series expansion over the parameter $e^{-R/a}$ [25]. The calculation shows that at large $q \gg \pi/R$ the form factor $F(q)$ corre-

sponding to the Woods-Saxon density profile goes to zero much faster than that for the homogeneous sphere distribution (33).

III. PAIR PRODUCTION BY BREMSSTRAHLUNG OF NUCLEAR MESON FIELDS

Taking into account only the first term in Eq. (30) and using Eqs. (15) and (21) one obtains the spectral distribution of $N\bar{N}$ pairs in the lowest order in the mean field

$$E_+E_-\frac{d^6N^{(1)}}{d^3p_+d^3p_-}=\frac{d_\tau}{2(2\pi)^6}\{(P^2-4m_N^2)|S(P)|^2$$
$$-P^2V_\mu^*(P)V^\mu(P)-4|Q_\mu V^\mu(P)|^2$$
$$-8m_N\,\mathrm{Re}[S^*(P)Q_\mu V^\mu(P)]\}. \quad (36)$$

Here

$$P=p_++p_-, \quad (37)$$

$$Q=\tfrac{1}{2}(p_+-p_-). \quad (38)$$

It is worth noting that Eq. (36) may be applied also to the lepton pair production by Coulomb fields of the colliding nuclei. To get the spectrum of e^+e^- pairs, it is sufficient to replace the baryonic current (12) by the electromagnetic one and make the substitutions

$$g_S\to0, \quad g_V\to\sqrt{4\pi}\,e, \quad m_N\to m_e, \quad m_\omega\to0, \quad d_\tau\to1, \quad (39)$$

where m_e and e are the mass and charge of the electron, respectively. The obtained expression for e^+e^- spectrum coincides with the corresponding formula of Ref. [10].

By using Eqs. (13), (31), and (32) one can write the following expressions for the Fourier transforms of J^μ:

$$J^0(P)=\frac{P_\parallel}{P_0}J^3(P)$$

$$=2A\int_{-\infty}^\infty dt\,e^{iP_0t}\cos[P_\parallel\xi(t)]$$

$$\times F(\sqrt{P_T^2+P_\parallel^2\cdot[1-\dot\xi^2(t)]}), \quad (40)$$

where $P_\parallel$ and $\boldsymbol{P}_T$ are, respectively, the longitudinal and transverse components of the three-momentum $\boldsymbol{P}$ in the e.v. frame. In the first equality we use the continuity equation for the baryon current and disregard the transverse components $\boldsymbol{J}_T$.

Several conclusions may be drawn already from Eq. (40). First, in the free-streaming limit ($\dot\xi=$ const) the bremsstrahlung radiation vanishes in the lowest order in the vector field. Indeed, in this case $\xi(t)$ is a linear function of t and according to Eq. (40) $J^\mu(P)\neq0$ only for $P_0=\pm P_\parallel\dot\xi$. This gives $P^2=P_\parallel^2(\dot\xi^2-1)-\boldsymbol{P}_T^2<0$ and, therefore, $V^\mu(P)=0$ in the region $P^2>0$. By using Eq. (40) one can estimate the region of the total three-momentum, $\boldsymbol{P}$, where $J^\mu(P)$ is essentially nonzero. Due to the presence of the form factor the characteristic momenta satisfy the relations

$$P_T\lesssim\frac{1}{R}, \quad |P_\parallel|\lesssim\frac{\gamma_0}{R}, \quad (41)$$

where $\gamma_0=(1-v_0^2)^{-1/2}$ is the initial Lorentz factor of nuclei. On the other hand, according to Eq. (40) $\lim_{P_\parallel\to0}J^\mu(P)=0$ at $P_0\neq0$. This leads to the suppression of pair production at small longitudinal total momenta in the e.v. frame. As we shall see below, this results in the two-hump structure of the bremsstrahlung component of the antibaryon rapidity distributions with a minimum at zero c.m. rapidity. The central dip appears as a result of destructive interference of the projectile and target contributions. The suppression of secondary particle yields at the emission angles $\theta_{c.m.}\simeq90°$ is a characteristic feature of the bremsstrahlung radiation in a symmetric nuclear collision. The analogous suppression was predicted earlier for the pion [15] and photon [10,11] bremsstrahlung.

Instead of the two-particle spectrum (36) let us consider first the distribution of pairs in their total momentum (37). Introducing the invariant mass $M\equiv\sqrt{P^2}$ of the $B\bar{B}$ pair, one may represent the components of P as

$$P_0=M_T\cosh Y, \quad P_\parallel=M_T\sinh Y, \quad (42)$$

where $M_T\equiv\sqrt{M^2+P_T^2}$ and Y is the rapidity of the $B\bar{B}$ pair center of mass.

Due to the mass shell constraint $p_\pm^2=m_N^2$ only two components of the four-vector Q, Eq. (38), are independent at given P. After integrating both parts of Eq. (36) over Q one obtains the result (see Appendix A)

$$\frac{d^4N^{(1)}}{d^4P}=\frac{d^4N^{(1)}}{M\,dM\,dY\,d^2P_T}$$

$$=\frac{d_\tau}{(2\pi)^5}\sqrt{1-\frac{4m_N^2}{M^2}}\Theta(M-2m_N)$$

$$\times\left\{\frac{M^2-4m_N^2}{2}|S(P)|^2\right.$$

$$\left.+\frac{M^2+2m_N^2}{3}|V_\mu^*(P)V^\mu(P)|\right\}. \quad (43)$$

From Eqs. (17), (19), (40), and (42), disregarding the transverse components J_T we get

$$|V_\mu^*(P)V^\mu(P)|\simeq\frac{g_V^4}{(M^2-m_\omega^2)^2}\left|\frac{J^0(P)}{\sinh Y}\right|^2. \quad (44)$$

Note that this expression has no singularity at $Y\to0$. Indeed, it can be shown from Eq. (40) that in this limit the vector density $J^0(P)$ vanishes more rapidly than $\sinh Y$. The pole at $M=m_\omega$ corresponds to the emission of the on-mass-shell ω mesons [20]. Since we are interested in the domain $M>2m_N>m_\omega$, there is no need for any regularization procedure. Of course, some interesting phenomena may occur when pairs are produced within dense baryonic matter. In this case a reduction of the nucleon effective mass m_N^* is predicted by the Walecka model [2], and therefore one may expect a situation when the gap $2m_N^*$ becomes less than

m_ω in the course of a nuclear collision. One can see that the decay channel $\omega \to B\bar{B}$ is opened under this condition. The consistent treatment of this effect is not possible within a simple perturbative scheme adopted here.

In the following we omit the contribution of the scalar field having in mind sufficiently high bombarding energies when the relation (27) holds. From Eqs. (43) and (44) we obtain

$$\frac{d^4N^{(1)}}{dM\,dY\,d^2P_T} = \mathcal{F}_V(M)\left|\frac{J^0(P)}{\sinh Y}\right|^2, \qquad (45)$$

where

$$\mathcal{F}_V(M) = \frac{d_\tau g_V^4}{3(2\pi)^5}\sqrt{M^2-4m_N^2}\frac{M^2+2m_N^2}{(M^2-m_\omega^2)^2}\,\Theta(M-2m_N). \qquad (46)$$

Applying the same approximations to Eq. (36) one gets

$$E_+E_-\frac{d^6N^{(1)}}{d^3p_+\,d^3p_-} = \frac{d^6N^{(1)}}{dy_+\,d^2p_{T+}\,dy_-\,d^2p_{T-}}$$
$$\simeq \frac{2d_\tau}{(2\pi)^6}(m_N^2+Q_T^2)|V_\mu^*(P)V^\mu(P)|, \qquad (47)$$

where $y_\pm \equiv \operatorname{arctanh}(p_\parallel/E)_\pm$ are the longitudinal rapidities of particles. The single particle spectra of the produced antibaryons are obtained from Eq. (47) by integrating over p_+. In the numerical calculation we use a smallness of the parameter P_T/m_N [see Eq. (41)]. This leads to the approximate relations

$$p_{T\pm} = \frac{P_T}{2} \pm Q_T \simeq \pm Q_T, \quad Y \simeq \frac{y_++y_-}{2}, \qquad (48)$$

$$M_T \simeq M \simeq 2\sqrt{m_N^2+Q_T^2}\,\cosh\frac{y_+-y_-}{2}. \qquad (49)$$

In this paper we adopt the Fermi-type parametrization of $\dot{\xi}(t)$ [10,14]:

$$\dot{\xi} = v_f + \frac{v_0-v_f}{1+e^{t/\tau}}, \qquad (50)$$

where τ is the effective deceleration time and $v_0(v_f)$ is the initial (final) velocity of nuclei in the e.v. frame. The deceleration law (50) describes the energy losses of the projectile and target nuclei during their mutual interpenetration. It contains two model parameters: τ and v_f. The total available c.m. energy per baryon at $t \to -\infty$ can be written as

$$\sqrt{s}/2A = m_N\gamma_0 = m_N\cosh y_0. \qquad (51)$$

Here $y_0 = \operatorname{arctanh} v_0$ and $\sqrt{s}$ are, respectively, the initial rapidity and total energy of nuclei in the e.v. frame. The degradation of energy in a nuclear collision can be characterized by the rapidity shift $\delta y = y_0-y_f$, where $y_f = \operatorname{arctanh} v_f$ is the final c.m. rapidity of the projectile. The study of rapidity spectra of leading nucleons in ultrarelativistic proton-nucleus

collisions shows [1,26] that δy is approximately independent of the bombarding energy and is determined mainly by the projectile path length in the target nucleus. Extrapolating this conclusion to the central collision of equal nuclei we may roughly estimate δy as a ratio of the nuclear radius R to the mean free path λ_N of a nucleon in nuclear matter. In the case of central Au+Au collisions at RHIC energy ($\sqrt{s}=200A$ GeV) the hydrodynamic [1,27] and RQMD [28] models predict mean rapidity losses $\delta y \simeq 2.4\pm 0.2$, which are close to the estimate mentioned above. Having this in mind we choose $\delta y \simeq 2.4$ for the heaviest combinations at $\sqrt{s} \gg 10A$ GeV. At lower energies (corresponding formally to $y_0-\delta y < 0$) we assume that the mutual stopping takes place at the final stage of the reaction, i.e., we put $v_f=0$ in Eq. (50).

According to Eq. (50) the nuclear deceleration, $\ddot{\xi}(t)$, is essentially nonzero within the time interval $-\tau < t < \tau$. Below it is assumed that 2τ is equal to the passage time in the e.v. frame, $2R/\gamma_0 v_0$. This leads to the following relations for the parameter τ:

$$\tau = R/\gamma_0 v_0 = R \cdot \left[\left(\frac{\sqrt{s}}{2m_NA}\right)^2 - 1\right]^{-1/2}. \qquad (52)$$

Of course, this ansatz is not correct at low energies when the full stopping of nuclei is reached in the collision. However, this will not cause a serious error since, as will be shown below, the bremsstrahlung mechanism gives a negligible pair yield at such energies.

The energy dependence of the bremsstrahlung contribution may be easily understood in some limiting cases when an analytic calculation of the Fourier transformed vector density $J^0(P)$ is possible. For example, this can be done in the case of instantaneous deceleration [$\ddot{\xi}(t) \propto \delta(t)$], when $\tau \to 0$. According to Eq. (52) this corresponds to the high energy limit $\sqrt{s} \to \infty$. Substituting

$$\xi = v_0 t\,\Theta(-t) + v_f t\,\Theta(t) \qquad (53)$$

into Eq. (40) we arrive at the expression

$$J^0(P) = 2iAP_0\left[\frac{F_0}{P_0^2-P_\parallel^2 v_0^2} - \frac{F_f}{P_0^2-P_\parallel^2 v_f^2}\right], \qquad (54)$$

where $(j=0,f)$

$$F_j \equiv F\left(\sqrt{P_T^2+P_\parallel^2/\gamma_j^2}\right) = F\left(\sqrt{P_T^2+M_T^2\sinh^2 Y/\cosh^2 y_j}\right). \qquad (55)$$

In the considered limit the pair spectra, Eqs. (45) and (47), are proportional to the factor

$$\left|\frac{J^0(P)}{\sinh Y}\right|^2 = \frac{A^2}{M_T^2\tanh^2 Y}\left|\frac{F_0\cdot(1+\cosh 2y_0)}{\cosh 2Y+\cosh 2y_0}\right.$$
$$\left. - \frac{F_f\cdot(1+\cosh 2y_f)}{\cosh 2Y+\cosh 2y_f}\right|^2. \qquad (56)$$

As one can see from Eqs. (54)–(56), the pair yield vanishes at the c.m. pair rapidity $Y \to 0$ and also in the free-streaming case $y_0-y_f \to 0$. According to Eq. (56) the Y dependence of spectra is determined mainly by the form factors $F_{0,f}$.

To analyze qualitatively the pair production at lower energies when the effective deceleration time is essentially nonzero we disregard the time dependence of the form factor in Eq. (40) replacing it by $F(P_T)$. This approximation may be justified for small enough values of $|P_{\parallel}|$ in the ultrarelativistic case $\dot{\xi} \simeq 1$. Determining $\xi(t)$ from Eq. (50) and calculating the integral in Eq. (40) one can easily get

$$J^0(P) = 2\tau A F(P_T)\{B[i\tau(P_0 + v_0 P_{\parallel}), -i\tau(P_0 + v_f P_{\parallel})]$$
$$+ B[i\tau(P_0 - v_0 P_{\parallel}), -i\tau(P_0 - v_f P_{\parallel})]\}, \qquad (57)$$

where $B(x,y) = \Gamma(x)\Gamma(y)/\Gamma(x+y)$ is the beta function. The same expression, but for the pointlike nuclei ($F = 1$), was obtained in Ref. [10]. In the limit $\tau \to 0$ we again arrive at Eq. (54) with $F_0 = F_f = F(P_T)$.

In the opposite case of large $P_0\tau$ the Fourier components $J^0(P)$ are essentially nonzero at $|Y| \simeq y_0, y_f$. The following approximate expression can be obtained at $P_0\tau \gg 1$ from Eq. (57):

$$\left|\frac{J^0(P)}{\sinh Y}\right|^2 \simeq \frac{8\pi\tau}{M_T}[AF(P_T)]^2 \tanh(y_0 - y_f) \sum_{j=0,f} \frac{1}{\sinh y_j}$$
$$\times \exp\left[-\frac{2\pi\tau M_T}{\cosh y_j} \cosh(|Y| - y_j)\right]. \qquad (58)$$

In deriving this expression we neglected the interference between two terms in Eq. (57) and assumed that $y_j \gtrsim 1$. From Eq. (58) one can see that the pair production by bremsstrahlung is exponentially small in the adiabatic region $P_0'\tau' \gg 1$, where $P_0' = M_T \cosh(Y \pm y_0)$ and $\tau' = \tau/\cosh y_0$ are, respectively, the total pair energy and the deceleration time in the projectile (target) rest frame. The above condition implies that the deceleration time is large as compared with the characteristic time, $(P_0')^{-1}$, necessary to produce a pair with energy P_0.

Let us estimate the bombarding energy at which the adiabatic regime sets in and the induced pair production becomes negligible. From Eq. (58) one can conclude that it is the case when $4\pi m_N\tau/\cosh y_0 \gg 1$. By using Eq. (52) we see that the adiabatic region is achieved when

$$\frac{\sqrt{s}}{A} \ll 4 m_N \sqrt{\pi m_N R} \sim \begin{cases} 40 \ \text{GeV}, & \text{Au+Au,} \\ 30 \ \text{GeV}, & \text{S+S.} \end{cases} \qquad (59)$$

Below the numerical calculations are made for these two cases of Au+Au and S+S central collisions.

Of course, this prediction should be regarded with care. Indeed, our treatment of the meson field dynamics is rather crude. In a real situation nuclei do not decelerate as a whole, but a compressed and excited matter is produced in the overlap region. Internal compression waves and shocklike fronts may be formed in the course of a nuclear collision.[2] It is clear that compression waves may lead to the local deceleration times which are shorter than the nuclear passage time. In this situation the Fourier frequencies, much higher than

τ^{-1}, may contribute to the pair production. A rough estimate may be obtained by replacing R in Eqs. (52) and (59) by a characteristic width of the compression wave λ. Assuming that $\lambda \sim \lambda_N \sim 1-2$ fm one can expect that the adiabatic boundary for the $N\bar{N}$ production may be shifted to the region of CERN SPS energies ($\sqrt{s}/A \simeq 19.4$ GeV). The reduction of the nucleon effective mass m_N^* in a dense matter [2] will also lead to the enhancement of the pair yield at all energies (see Sec. VI). As compared to Eq. (59) the adiabatic threshold will be lowered in accordance with the factor $(m_N^*/m_N)^{3/2}$.

IV. PAIR PRODUCTION BY FUSION OF VIRTUAL ω MESONS

In this section we study the $B\bar{B}$ production by processes of the second order in the mean-field interaction [see Fig. 1(b)]. As has been already stated, in this case pairs may be produced even if the deceleration of nuclei is disregarded. To avoid complications connected with mutual slowing down of the colliding nuclei, below the second order processes will be studied in the free-streaming limit. As will be shown, the contribution of these processes drops with decreasing relative energy of nuclei. Therefore we expect that the neglect of nuclear deceleration overestimates the magnitude of the second order effects.

In the free-streaming approximation, $\dot{\xi} = v_0 = $ const, the four-velocities of nuclei, $U_\mu^{(\alpha)}$ are constant. As seen from Eq. (32), in this case the time dependence of nuclear densities enters in the combination $z - v_0 t$ only. Using Eqs. (13), one can represent the Fourier components of the vector field as

$$V_\mu(k) = \sum_{\alpha = p,t} V_\mu^{(\alpha)}(k), \qquad (60)$$

where

$$V_\mu^{(\alpha)}(k) = -D_V(k)\rho_V^{(\alpha)}(k)U_\mu^{(\alpha)}. \qquad (61)$$

Here the Fourier transformed vector densities of the projectile ($\alpha = p$) and target ($\alpha = t$) nuclei can be expressed via the nuclear form factor [see Eq. (34)]

$$\rho_V^{(\alpha)}(k) = 2\pi\delta(kU^{(\alpha)}) \cdot AF(\sqrt{-k^2}). \qquad (62)$$

Under the constraint imposed by the δ-function, $k_0 = \pm k_{\parallel} v_0$, the components of the four-vector k satisfy the relation

$$k^2 = -k_{\perp}^2 - \frac{k_{\parallel}^2}{\gamma_0^2} < 0, \qquad (63)$$

where $k_{\perp}$ are the transverse components of k. Therefore, only the spacelike momenta k of the vector field contribute in this case.

As before we disregard the contribution of the scalar meson field. Then the term of the second order in Eq. (30) can be written as

---

[2]The photon bremsstrahlung in the case of a shock wave excitation has been considered in Refs. [29,30].

$$\mathscr{B}^{(2)}(p_+,p_-)=\int\int\frac{d^4k_1d^4k_2}{(2\pi)^8}(2\pi)^4$$

$$\times\delta(k_1+k_2-p_+-p_-)V_\mu^{(p)}(k_1)V_\nu^{(t)}(k_2)$$

$$\times H^{\mu\nu}(k_1,p_+,p_-).\qquad(64)$$

Here $H^{\mu\nu}$ is the hadronic tensor (the operator in bispinor indices)

$$H^{\mu\nu}(k_1,p_+,p_-)=\gamma^\mu G(p_+-k_1)\gamma^\nu+\gamma^\nu G(k_1-p_-)\gamma^\mu,\qquad(65)$$

where the first and second terms correspond to the left and right diagrams in Fig. 1(b). By using Eqs. (29) and (64) it can be shown that the second order matrix element is invariant under the gauge transformation of the vector fields

$$V_\mu^{(\alpha)}(k)\rightarrow V_\mu^{(\alpha)}(k)+Ck_\mu,\qquad(66)$$

where C is an arbitrary scalar function of k. The latter can be chosen so that only the transverse components $\mu,\nu=1,2$ contribute to the operator (64) [9].

The conditions $k_1U^{(p)}=k_2U^{(t)}=0$ and the four-momentum conservation $k_1+k_2=p_++p_-\equiv P$ fix the components k_j^0 and k_j^3 ($j=1,2$):

$$k_1=\left(\omega_1,k_{1\perp},\frac{\omega_1}{v_0}\right),\qquad(67)$$

$$k_2=\left(\omega_2,k_{2\perp},-\frac{\omega_2}{v_0}\right).\qquad(68)$$

Here $k_{j\perp}$ are the transverse components of k_j and

$$\omega_1=\tfrac{1}{2}(P_0+v_0P_\parallel)\simeq m_T(e^{y_+}+e^{y_-})\simeq\tfrac{1}{2}Me^Y,\qquad(69)$$

$$\omega_2=\tfrac{1}{2}(P_0-v_0P_\parallel)\simeq m_T(e^{-y_+}+e^{-y_-})\simeq\tfrac{1}{2}Me^{-Y},\qquad(70)$$

where $m_T\equiv\sqrt{m_N^2+Q_T^2}$. In deriving Eqs. (69) and (70) we used formulas (42) and (49) of the preceding section.

In Refs. [9,12] the method of equivalent photons [13,31] was applied to study the impact parameter dependence of the electromagnetic production of lepton pairs in relativistic nuclear collisions. In this paper we generalize this method and the procedure suggested in Refs. [9,12] for the case of "equivalent" ω mesons. In the lowest order approximation in the parameters γ_0^{-1} and $k_\perp/m_N\lesssim1/m_NR$ one can obtain the following expression for the differential spectrum of $N\overline{N}$ pairs in a central collision of equal nuclei (see Appendix B):

$$\frac{dN^{(2)}}{d\omega_1d\omega_2dt}=\int d^2r_\perp n(\omega_1,r_\perp)n(\omega_2,r_\perp)\frac{d\sigma(s)}{dt}.\qquad(71)$$

Here $n(\omega,r_\perp)$ is the spectral distribution of virtual ω mesons at the distance $r_\perp$ from the beam axis. The term $d\sigma(s)/dt$ denotes the differential cross section of the reaction[3]
$\omega(k_1)+\omega(k_2)\rightarrow N(p_+)+\overline{N}(p_-)$.

---

[3]The four-momenta of particles are given in parentheses. For example, $\omega(k_j)$ denotes the virtual ($k_j^2\simeq0$) vector meson with the momentum k_j.
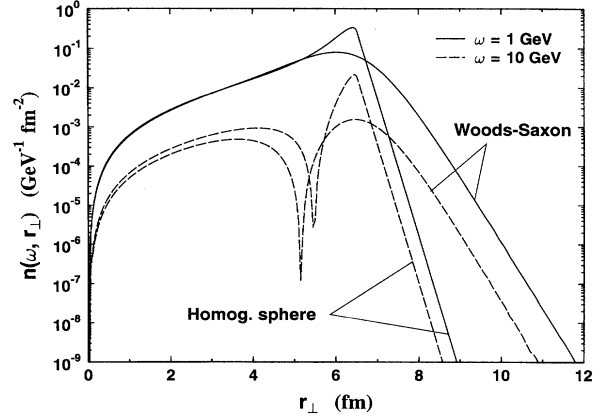

FIG. 3. Spectral density of virtual vector mesons for gold nucleus as function of distance $r_\perp$ from the beam axis ($\sqrt{s}=200A$ GeV). Solid and dashed lines correspond to the meson energy $\omega=1$ and 10 GeV in the equal velocity frame.

This cross section corresponds to the case of parallel polarizations [12] of equivalent vector mesons and depends on the Mandelstam variables

$$s=(k_1+k_2)^2=M^2\simeq4\omega_1\omega_2,\qquad(72)$$

$$t=(p_+-k_1)^2.\qquad(73)$$

The explicit formula for the "ω-fusion" cross section may be written as [see Eq. (B8) in Appendix B]

$$\frac{d\sigma(s)}{dt}=\sigma_0\cdot\frac{4m_N^2}{s^2}\left[\frac{s/2+2m_N^2}{m_T^2}-1-\frac{3m_N^4}{m_T^4}\right],\qquad(74)$$

where $\sigma_0=d_rg_V^4/16\pi m_N^2$.

The function $n(\omega,r_\perp)$ describes the flux density of mesons with the energy ω created by a nucleus moving with the velocity v_0. It can be expressed as

$$n(\omega,r_\perp)=\frac{(Ag_V)^2}{\pi\omega}\left|\int\frac{d^2k_\perp}{(2\pi)^2}k_\perp e^{ik_\perp r_\perp}\frac{F(\sqrt{k_\perp^2+\omega^2/\gamma_0^2v_0^2})}{k_\perp^2+\omega^2/\gamma_0^2v_0^2+m_\omega^2}\right|^2.\qquad(75)$$

The corresponding distribution of photons may be obtained by replacing $Ag_V\rightarrow Z\sqrt{4\pi}e$, $m_\omega\rightarrow0$. Unlike the case of the electromagnetic field, $n(\omega,r_\perp)$ decreases exponentially with $r_\perp$ at $r_\perp>R$ (see Fig. 3). This is a consequence of the short-range nature of nuclear meson fields.

The pair spectra in terms of "observable" kinematic variables $y_\pm,Q_T\simeq p_{T\pm}$ may be obtained from Eq. (71) by using the relation [see Eqs. (69) and (70)]

$$d\omega_1d\omega_2dt=\frac{s}{4}dy_+dy_-dm_T^2.\qquad(76)$$

Various equivalent representations of Eqs. (71) and (74) can be written by applying the approximate kinematic formulas

$$m_N^2-t=\frac{s}{1+e^{y_+-y_-}}=m_T^2(1+e^{y_--y_+}).\qquad(77)$$

From Eq. (71) one can easily get the second order (ω-fusion) contribution to the $\overline{N}N$ multiplicity, $N_{\text{pair}}^{(2)}$. A straightforward calculation gives

$$N_{\text{pair}}^{(2)} = \int d^2 r_\perp \int_0^\infty d\omega_1 n(\omega_1, r_\perp) \int_0^\infty d\omega_2 n(\omega_2, r_\perp) \sigma(s).$$

$$(78)$$

Here $\sigma(s)$ is the total $\omega\omega \to N\overline{N}$ cross section

$$\sigma = \sigma_0 x \left[\left(1 - x - \frac{3x^2}{4} \right) \ln \frac{1 + \sqrt{1-x}}{1 - \sqrt{1-x}} - \left(1 + \frac{3x}{4} \right) \sqrt{1-x} \right]$$

$$\times \Theta(1 - x),$$

$$(79)$$

where $x = m_N^2 / \omega_1 \omega_2$. The corresponding antiproton multiplicity is obviously a half of that given by Eq. (78). The analogous formula for the electromagnetic case may again be obtained by substitutions (39) and $A \to Z$.

V. DIRECT PRODUCTION OF $N\overline{N}$ PAIRS IN BINARY NUCLEON-NUCLEON COLLISIONS

In this section we estimate the contribution of the direct pair production in binary collisions of nucleons. We use the conventional convolution model assuming that antinucleons are produced as a result of incoherent superposition of the NN collisions, in accordance with the experimentally observed $NN \to \overline{N}X$ cross section. Due to the high threshold of the $NN \to \overline{N}X$ reaction ($\sqrt{s}_{\text{thr}} = 4m_N \simeq 3.754$ GeV) we take into account only the projectile-target nucleon collisions.

We proceed from the same scenario of nuclear interpenetration as considered in Secs. II and III. Disregarding the dispersion of the nucleon momentum distribution, the spectrum of the directly produced antinucleons can be written as follows[4]:

$$\frac{d^3 N_{\overline{N}}^{(\text{dir})}}{d^3 p} = \int d^4 x \; \rho_V^{(p)}(x) \rho_V^{(t)}(x) \sqrt{[U^{(p)}(x) U^{(t)}(x)]^2 - 1}$$

$$\times \frac{d^3 \sigma_{NN \to \overline{N}X}}{d^3 p} \Bigg|_{s = m_N^2 [U^{(p)} + U^{(t)}]^2}.$$

$$(80)$$

Here the same notations are used as in Eqs. (31) and (32) and $d\sigma_{NN \to \overline{N}X}/d^3 p$ is the differential cross section of the $NN \to \overline{N}X$ reaction at the c.m. energy squared s.

In the standard convolution model deceleration effects are disregarded. In this free-streaming case the four-velocities $U^{(\alpha)}$ are constant and the densities $\rho^{(\alpha)}$ are functions of $r_\perp$ and $z \pm v_0 t$. A straightforward calculation of the integral in Eq. (80) gives the following result in the case of a nuclear collision at the impact parameter b:

$$\frac{d^3 N_{\overline{N}}^{(\text{dir})}}{d^3 p} = T(b) \frac{d^3 \sigma_{NN \to \overline{N}X}}{d^3 p} \Bigg|_{s = s_0}.$$

$$(81)$$

---

[4]The analogous expression in the case of pion production has been suggested in Ref. [32].

Here $\sqrt{s}_0 = 2m_N \gamma_0$ is the initial energy (per baryon) in the e.v. frame, $T(b)$ is the overlap integral

$$T(b) = \int d^2 r_\perp l_p(|r_\perp - b|) l_t(r_\perp),$$

$$(82)$$

where $l_\alpha(r_\perp)$ is the longitudinal "thickness" of the nucleus $\alpha = p, t$:

$$l_\alpha(r_\perp) = \int_{-\infty}^\infty dz \rho_\alpha(\sqrt{r_\perp^2 + z^2}).$$

$$(83)$$

The rough estimates may be obtained assuming the homogeneous sphere density distribution and using the $pp \to \overline{N}X$ data instead of the isospin-averaged $NN \to \overline{N}X$ cross section. In the case of a central collision between equal nuclei $T(0) = 9A^2 / 8\pi R^2$ and we get the simple expression for the total multiplicity of direct antiprotons

$$N_{\overline{p}}^{(\text{dir})} = \frac{9}{8} \frac{A^2}{\pi R^2} \sigma_{pp \to \overline{p}X} \Bigg|_{s = s_0} \simeq 0.026 A^{4/3} \sigma_{pp \to \overline{p}X} (\text{mb}),$$

$$(84)$$

where $\sigma_{pp \to \overline{p}X}$ is the total cross section of the inclusive process $pp \to \overline{p}X$.

Due to the neglect of deceleration the predictions of the standard convolution model, Eq. (84), should be regarded as an upper bound. We have modified the convolutional model by implementing the mutual slowing down of nuclei according to the deceleration law suggested in Eq. (50). From Eq. (80), assuming the homogeneous density distribution, we get the relation generalizing Eq. (84) for this case

$$N_{\overline{p}}^{(\text{dir})} = \int_{-\infty}^\infty dt \, \nu_{NN}(t) V_{\text{over}}(t) \sigma_{pp \to \overline{p}X} \Bigg|_{\sqrt{s} = 2m_N \gamma(t)}.$$

$$(85)$$

Here $\nu_{NN} = 2\rho_0^2 \gamma^2 |\dot\xi|$ is a quantity proportional to the frequency of elementary NN collisions, $\dot\xi$ and γ are, respectively, the velocity of the projectile center and the corresponding Lorentz factor in the e.v. frame, V_{over} is the volume of the projectile-target geometric overlap

$$V_{\text{over}} = \int d^3 r \Theta(R^2 - r_\perp^2 - \gamma^2 (|\xi| + |z|)^2)$$

$$= \frac{2\pi}{3\gamma} (R - \gamma|\xi|)^2 (2R + \gamma|\xi|) \Theta(R - \gamma|\xi|).$$

$$(86)$$

It is easy to verify that in the free-streaming limit ($\dot\xi = v_0$) Eqs. (85) and (86) give the same $\overline{p}$ multiplicity as Eq. (84).

To calculate the excitation function of direct antiprotons one should know the energy dependence of $\sigma_{pp \to \overline{p}X}$. In the region $\sqrt{s}_{\text{thr}} < \sqrt{s} < 15$ GeV we use the parametrization of experimental data suggested in Ref. [33]:

$$\sigma_{pp \to \overline{p}X} = 0.012(\sqrt{s} - 4m_N)^{1.846}.$$

$$(87)$$

Here and below $\sqrt{s}$ and $\sigma_{pp \to \overline{p}X}$ are given in GeV and mb, respectively. In the high energy domain the $pp \to \overline{p}X$ data are usually represented in terms of the average $\overline{p}$ multiplicity in a single pp collision, $\langle n_{\overline{p}} \rangle \equiv \sigma_{pp \to \overline{p}X} / \sigma_{pp}^{\text{in}}$, where σ_{pp}^{in} is the
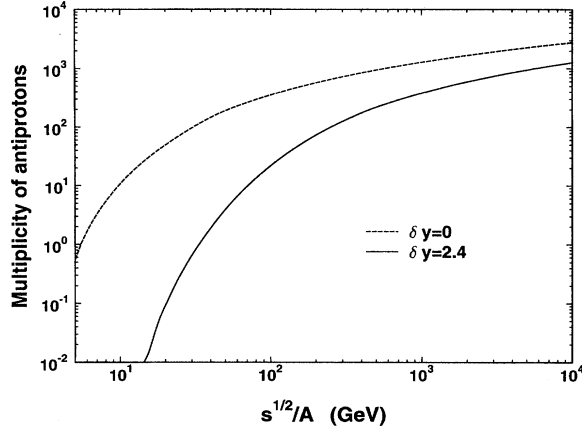
FIG. 4. Multiplicity of direct antiprotons in central Au+Au collisions as a function of c.m. bombarding energy per nucleon. Dashed line shows the result of calculation in the free-streaming approximation. Solid line is calculated with inclusion of deceleration effects assuming the rapidity loss $\delta y = 2.4$.

inelastic pp cross section. At $50 < \sqrt{s} < 10^4$ we use the average of the two parametrizations of the ISR and FNAL data given in Ref. [34]:

$$\langle n_{\bar{p}} \rangle = -0.7 + \frac{0.37}{\sqrt{s}} + \left(0.1 + \frac{0.5}{\sqrt{s}} \right) \ln s. \qquad (88)$$

Multiplying this function by the inelastic cross section ($50 \lesssim \sqrt{s} \lesssim 10^4$)

$$\sigma_{pp}^{in}(\text{mb}) = 5.1 + 7.5 \ln \sqrt{s}, \qquad (89)$$

we obtain the high energy approximation of $\sigma_{pp \to \bar{p}X}$. At the intermediate energies $15 < \sqrt{s} < 50$ we apply a powerlike decomposition

$$\sigma_{pp \to \bar{p}X} = \sum_{i=0}^{3} a_i s^{i/2}, \qquad (90)$$

matching smoothly with the parametrizations (87) and (88) and (89). The matching procedure gives the values $a_0 = -0.3663$, $a_1 = 3.816 \times 10^{-2}$, $a_2 = 3.503 \times 10^{-3}$, and $a_3 = -3.609 \times 10^{-5}$.

The results of numerical calculation based on Eqs. (84) and (85) are shown in Fig. 4 for the case of central Au+Au collisions. We use the deceleration law (50) with the same parameters τ and δy as suggested in Sec. III. One can see that due to the degradation of energy (mutual stopping) of baryons in the course of the nuclear collision, the direct $\bar{p}$ yield is strongly reduced as compared with the free-streaming case.

VI. RESULTS

Below we present the results of numerical calculations obtained within the model described in the preceding sections. We adopt the following parameters of the vector meson interaction [36]

$m_\omega = 0.783$ GeV, $g_V = 13.78$, $\Lambda_V = 2$ GeV. (91)

These values are in a good agreement with the parameters used in the OBEP potentials [37] as well as in the realistic mean-field models (see Ref. [38]). One should bear in mind, however, that the antinucleon yields predicted by the considered coherent mechanism are rather sensitive to the choice of g_V. Indeed, as one can see from Secs. III and IV the contributions of bremsstrahlung and ω-fusion processes are proportional to g_V^4 and g_V^8, respectively. The results for other choices of g_V may be obtained by a simple rescaling of the antibaryon yields given in this section. The situation is even more uncertain in the case of the $\Lambda\bar{\Lambda}$ production. The corresponding formulas may be obtained from those in the $N\bar{N}$ case by replacing $m_N \to m_\Lambda$, $g_V = g_{VN} \to g_{V\Lambda}$. In this work we choose [38]

$$g_{V\Lambda} = \tfrac{2}{3} g_{VN} \qquad (92)$$

and assume the same cutoff mass Λ_V as for nucleons. The reduction of the coupling constant is the main reason for a noticeable suppression of the $\bar{\Lambda}$ yield as compared to the $\bar{p}$ production (see Figs. 9 and 13). Below we consider only central collisions of equal nuclei, namely, Au+Au and S+S reactions at various c.m. bombarding energies $\sqrt{s}$. Unless otherwise stated we use the Woods-Saxon density distribution and choose the deceleration time τ in accordance with Eq. (52). We assume the rapidity shifts $\delta y = 2.4$ (see Sec. III) and 1.6 [39] for the Au+Au and S+S central collisions, respectively.

Another physical quantity, which may enhance significantly the $B\bar{B}$ yields, is the baryon (antibaryon) effective mass $m_B^*(B=N,\Lambda, \ldots)$ [6,33]. Generally speaking, the reduction of m_B^* as expected in a dense medium should be determined self-consistently, by the space and time dependent scalar field, $m_B^* = m_B - g_{SB}\sigma$. But this study is out of the scope of this paper. Here we perform the calculations with constant m_B^*, which, however, can differ from the vacuum values m_B. In particular, for nucleons we take the value $m_N^* = 0.7 m_N$ attributed to normal nuclei. This choice might be not so unreasonable because pairs are produced predominantly in the space-time domain where the vector field has the strongest variation, i.e., within the colliding nuclei. The newly produced particles and the compression of matter may further increase the scalar density and, therefore, reduce m_B^*. To partly simulate these effects we also give results for $m_N^* = 0.5 m_N$.[5]

Figure 5 shows the antiproton multiplicity as a function of the bombarding energy (excitation function) in the case of central Au+Au collisions. The contributions of the bremsstrahlung and ω-fusion processes were calculated using Eqs. (45) and (78), respectively. To get the $\bar{p}$ multiplicity we put $d_\tau = 1$. Note that the ω-fusion component is calculated in the

_____

[5]One should be cautious using the formulas of Sec. III when $2m_N^*$ comes close to m_ω, i.e., to the pole of the ω-meson propagator. To regularize this pole, it is necessary to introduce the ω-meson width and to take into account the mixing of the ω and $N\bar{N}$ emission channels.
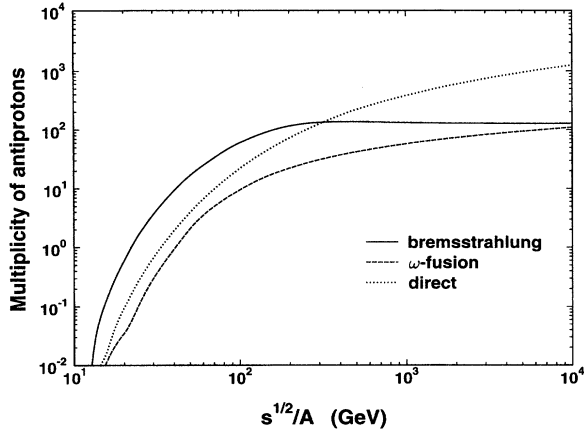
FIG. 5. Antiproton multiplicity in central Au+Au collisions versus c.m. bombarding energy per baryon. Solid and long dashed show the bremsstrahlung and ω-fusion contributions. Dotted line represents the direct $\bar{p}$ yield.
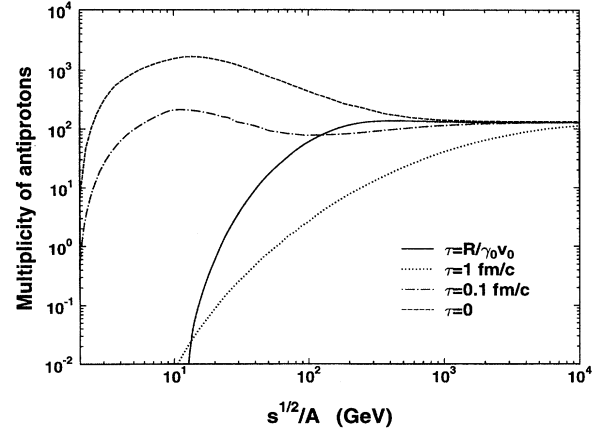

FIG. 7. Excitation function of antiprotons produced by bremsstrahlung in central Au+Au collisions. Solid line corresponds to the deceleration time τ equal to half of the passage time. Dotted and dashed-dotted lines are calculated for constant deceleration times $\tau=1$ and 0.1 fm/c. Dashed line corresponds to the instantaneous deceleration ($\tau=0$).

free-streaming approximation. For comparison we show also the direct $\bar{p}$ yield evaluated on the basis of Eq. (85). As one can see from Fig. 5, at all energies from AGS ($\sqrt{s}\simeq 5A$ GeV) to LHC ($\sqrt{s}=6.4A$ TeV) the ω-fusion process gives a smaller relative contribution as compared to the bremsstrahlung mechanism. The relative smallness of the second order contribution justifies to some extent the perturbative scheme used in our model. In accordance with the discussion given in Sec. III, the bremsstrahlung part of the antiproton multiplicity raises rapidly with $\sqrt{s}$ reaching the maximum, $N_{\bar{p}}^{\max}\sim 150$, near the RHIC energy and remains approximately constant at higher $\sqrt{s}$. At all energies below the RHIC domain the bremsstrahlung mechanism gives the $\bar{p}$ multiplicities greater or of the same order as the direct production mechanism.

In Fig. 6 we show the total c.m. energy E_{pair} of the $N\bar{N}$ pairs, produced by bremsstrahlung in the same reaction. This quantity was calculated by integrating the r.h.s. of Eq. (45)

with the weighting factor P_0. In the case of the vacuum nucleon mass, E_{pair} is about 10% of the available c.m. energy, $\sqrt{s}-2m_N A$. By comparing E_{pair} with the total mass of pairs, $2m_N N_{\mathrm{pair}}$, one can estimate an average kinetic energy of the $N\bar{N}$ pairs. E_{pair} may increase even more when $m_N^*<m_N$. These energy losses will modify significantly the stopping power of nuclear matter.

Figure 7 shows the sensitivity of the results to the choice of the model parameter τ characterizing the mutual deceleration of nuclei. One can see that the bremsstrahlung contribution is very sensitive to this choice and, therefore, may serve as a probe of the hadronic matter dynamics in nuclear collisions. However, Fig. 7 shows that at very high bombarding energies ($\sqrt{s}\gtrsim 500A$ GeV for central Au+Au collisions) the $\bar{p}$ multiplicities may be obtained with a good accuracy by assuming instantaneous mutual deceleration, $\tau\simeq 0$.

The A dependence of the bremsstrahlung pair production is illustrated in Fig. 8. As mentioned above, we expect

FIG. 6. Total c.m. energy E_{pair} of $N\bar{N}$ pairs produced by bremsstrahlung in central Au+Au collisions (solid line). Dotted and dashed lines correspond to total available energy, $\sqrt{s}-2m_N A$ and total mass of pairs, $2m_N N_{\mathrm{pair}}$, respectively.
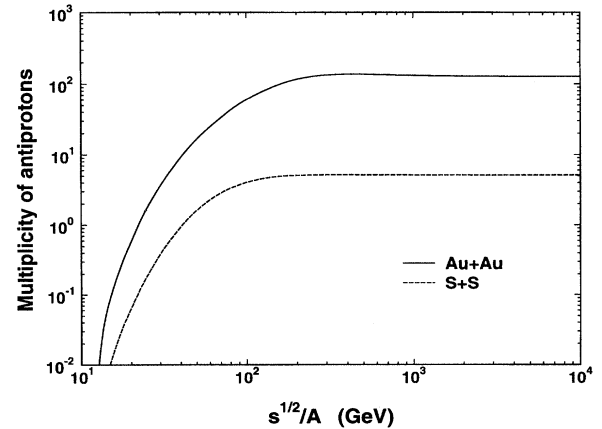

FIG. 8. Excitation functions of antiprotons (bremsstrahlung contribution) in central Au+Au and S+S collisions.
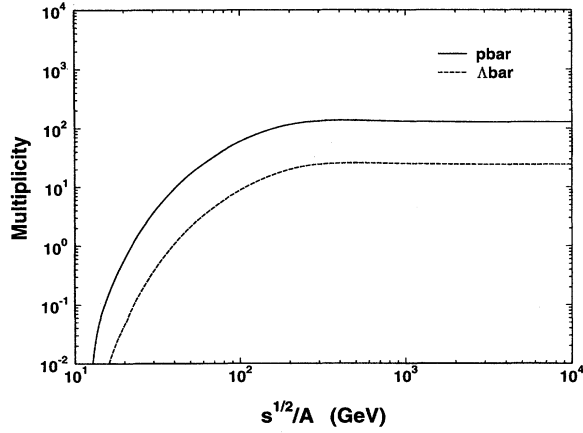
FIG. 9. Excitation functions of antiprotons (solid line) and anti-lambdas (dashed line) produced by the bremsstrahlung mechanism in central Au+Au collisions.

smaller values of the parameters τ and δy for the lighter combination S+S. But the factor A^2 [see Eqs. (40) and (45)] leads to a substantial suppression of $\bar{p}$ yields in the S+S reaction as compared to the Au+Au case.
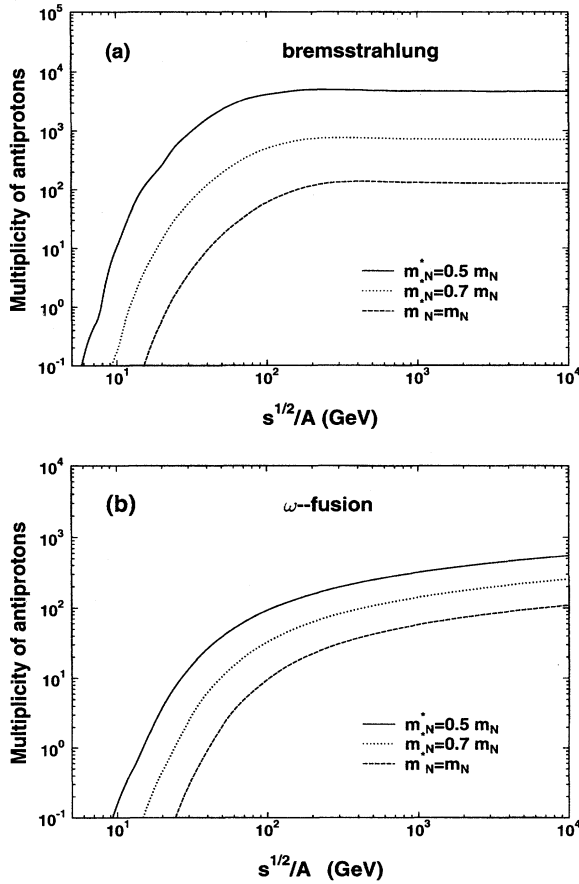

FIG. 10. Excitation functions of antiprotons in central Au+Au collisions produced by the bremstrahlung (a) and ω fusion (b) mechanisms. Results are shown for three different values of the nucleon effective mass m_N^*.
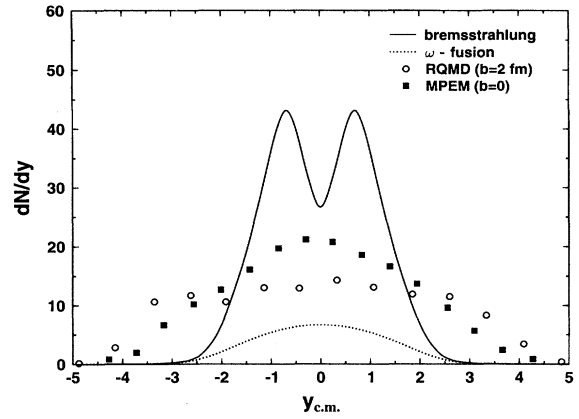
FIG. 11. Antiproton rapidity distribution in central Au+Au collisions at RHIC bombarding energy. Solid line represents the bremsstrahlung contribution. Dotted line shows the contribution of the ω fusion. Squares and diamonds show the results of RQMD (impact parameter $b=2$ fm) [27] and MPEM (multiparton eikonal model) [35].

The $\bar{p}$ and $\bar{\Lambda}$ bremsstrahlung yields are compared in Fig. 9. One can see that in the case of central Au+Au collisions the model predicts about a factor 5 smaller multiplicities of $\bar{\Lambda}$ than $\bar{p}$.

Figures 10(a) and (b) show the sensitivity of antiproton multiplicities to the choice of the nucleon effective mass. One can see that the reduction of m_N^* leads to a very pronounced enhancement of the antiproton yields, for both the bremsstrahlung [Fig. 10(a)] and ω-fusion [Fig. 10(b)] contributions. In accordance with the discussion of the adiabatic limit in Sec. III, this effect is especially pronounced at lower bombarding energies.

The rapidity and transverse momentum spectra of antibaryons at the RHIC energy are displayed in Figs. 11–16. The relative smallness of the ω-fusion contribution is once again demonstrated in Fig. 11. One can see that in the considered reaction the model predicts a clear dip of $dN_{\bar{p}}/dy$ at
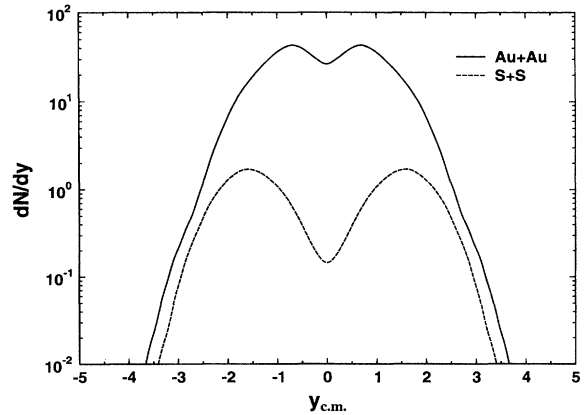

FIG. 12. Antiproton rapidity spectra in central Au+Au (solid line) and S+S (dotted line) collisions at RHIC energy $\sqrt{s}=200A$ GeV. Only bremsstrahlung contributions are shown. The rapidity shifts are $\delta y=2.4$ (Au+Au) and 1.6 (S+S).
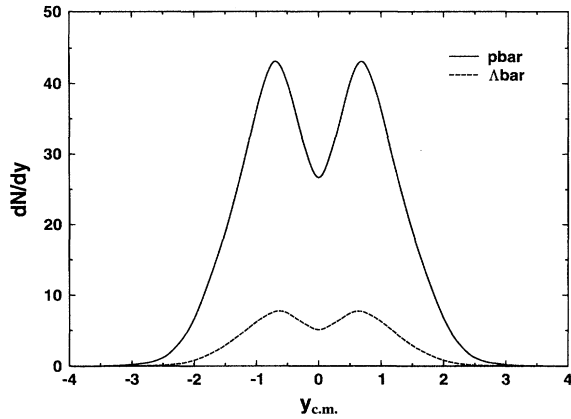
FIG. 13. Rapidity spectra of antiprotons (solid line) and anti-lambdas (dashed line) produced by the bremsstrahlung mechanism in central Au+Au collisions at RHIC energy.

midrapidity. This minimum becomes more pronounced for the lighter combination S+S (see Fig. 12) and is present also in the $\bar{\Lambda}$ spectra (Fig. 13). The two-hump structure of the antibaryon rapidity spectra is a result of the destructive interference between the projectile and target contributions discussed in Sec. III (the pair yield vanishes at the total pair rapidity $Y_{c.m.}=0$). These two peaks are separated only by two units of rapidity and have nothing to do with the conventional baryon peaks in the projectile and target rapidity region ($y_{c.m.} \simeq \pm 5$ at the RHIC energy). The appearance of the dip of $dN_{\bar{p}}/dy$ at midrapidity may be used as a clear signal of the bremsstrahlung mechanism. Indeed, at the same bombarding energy and the same combination of nuclei the models, assuming an incoherent particle production in binary collisions of nucleons or partons, predict much smoother and broader rapidity distributions of antibaryons. The results of the RQMD [28] and multiparton eikonal model (MPEM) [35] are also shown in Fig. 11. Of course, the annihilation processes may diminish to some extent the number of anti-protons, but in contrast, the reduced nucleon effective mass may enhance their yield (see the discussion in Sec. VII).

FIG. 15. Same as in Fig. 14, but for different values of rapidity shift δy.

Therefore, we expect that the nontrivial structure of antibaryon spectra may still be observable at high enough incident energies above the "background" of the direct production.

Figures 14 and 15 show how the shapes of the antiproton rapidity spectra depend on the parameters τ and δy charac-
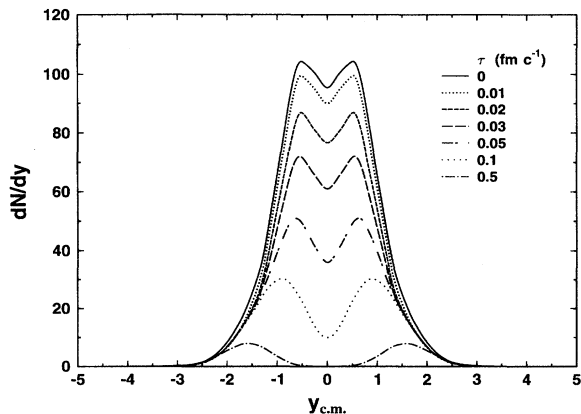

FIG. 14. Antiproton rapidity spectra in central Au+Au collisions at RHIC bombarding energy for different values of deceleration time. In all cases the rapidity shift $\delta y = 2.4$ is assumed.
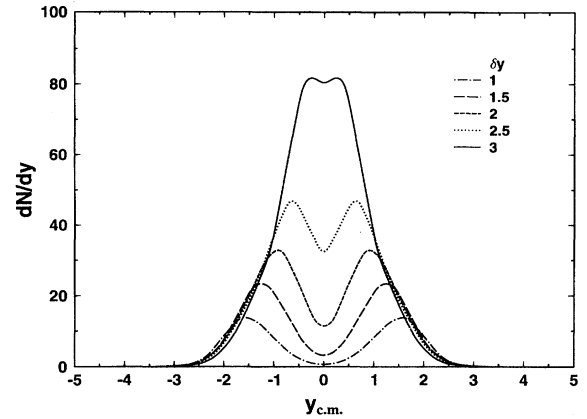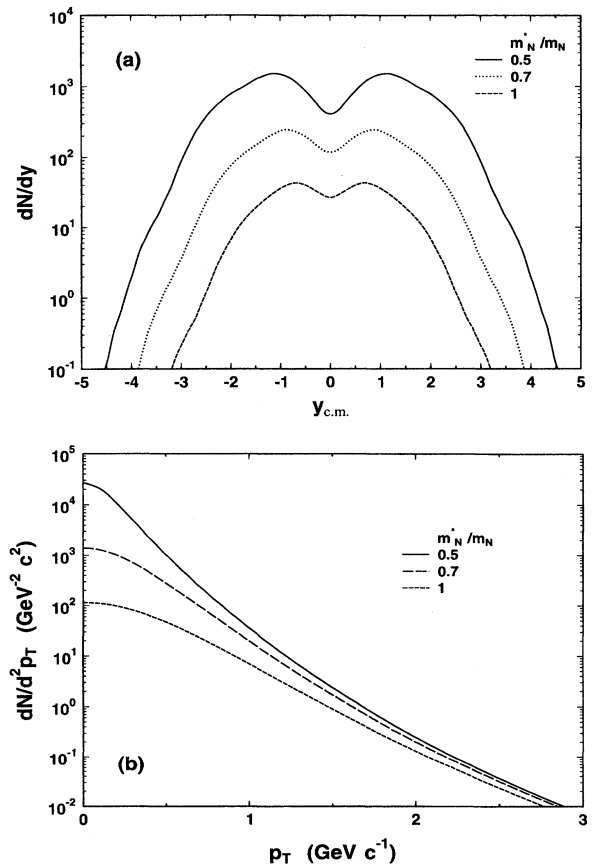

FIG. 16. Rapidity (a) and transverse momentum (b) spectra of antiprotons produced by the bremsstrahlung mechanism in central Au+Au collisions at RHIC energy. Results are shown for three different choices of the nucleon effective mass m_N^*.

terizing the global dynamics of the nuclear collision process. As before, one can see a high sensitivity of the bremsstrahlung production to the dynamics of baryon stopping. Only at very small τ, i.e., close to the limit of the instantaneous velocity loss, the spectra become independent on τ (Figs. 7, 14) This behavior was found earlier in the pion bremsstrahlung [14].

The sensitivity of differential spectra to the nucleon effective mass is demonstrated in Figs. 16(a) and (b). One can see that the reduction in the nucleon effective mass results in a significant enhancement of dN/dy at all rapidities [Fig. 16(a)]. In contrast the transverse momentum spectra are affected mostly at $p_T \lesssim m_N^*$ [Fig. 16(b)]. The calculations show the same qualitative behavior of differential spectra at the SPS and LHC energies.

VII. DISCUSSION AND CONCLUSIONS

In this paper we have demonstrated the importance of the coherent dynamical mechanism of the baryon-antibaryon pair production via the bremsstrahlung and the meson-meson fusion. Our calculations have a qualitative character aimed to emphasize the new features which are not present in thermal, fluid-dynamical, or cascade models. Within the perturbative approach we have shown that this new mechanism can give more antibaryons than the direct production in elementary nucleon-nucleon collisions. The collective mechanisms of pair production become important in central collisions of heavy nuclei at c.m. energies $\sqrt{s} \gtrsim 100A$ GeV, i.e., in the RHIC and LHC energy domains. In all considered cases the bremsstrahlung (first order) process gives a much larger contribution as compared to the ω fusion (second order) component.

It has been demonstrated that the coherent production is very sensitive to the dynamics of a heavy-ion collision. In particular, the bremsstrahlung mechanism leads to the two–hump structure of the antibaryon rapidity spectra, unlike the predictions of cascade models. The position of the peaks is related to the average rapidity loss of baryons in the deceleration process. Therefore, the experimental observation of this structure may give an additional information about the stopping power of nuclear matter.

Our schematic treatment ignores the back reaction (appearance of induced currents) of produced baryons and antibaryons. Apparently, this is a rather crude approximation. In the future one should implement a more realistic treatment of the source terms for meson fields taking into account the deformation of nuclear densities in the course of the reaction as well as the effects of the induced antibaryonic currents. Another obvious problem is to introduce the annihilation channels which will reduce the observable baryon yields. Two channels should be considered: first, the annihilation on the baryons of the colliding nuclei and, second, the annihilation between partners of different $B\bar{B}$ pairs. We expect that the first process is more important at lower energies (AGS and SPS) when the central rapidity region is strongly contaminated by stopped baryons. The cascade calculations show that in this case the annihilation effects could give large suppression factors (up to 30 for the AGS energy [40]). At higher energies, including the RHIC and LHC domain, this first channel is presumably not so strong and the annihi-

lation between the different $B\bar{B}$ pairs should be more important.

Rather high $B\bar{B}$ multiplicities are obtained in the model, especially when the reduction of the baryon effective mass is taken into account. For instance, thousands of coherent $N\bar{N}$ pairs are predicted in the heaviest combinations at RHIC energies. Of course, these large numbers should be considered with caution and only as an indication of possible orders of magnitude. Indeed, many uncertain factors, like the annihilation and vertex corrections, may reduce these numbers by a factor 10 or more. The realistic treatment of the nuclear collision dynamics is also necessary for more firm predictions. But despite these uncertainties the discussed coherent mechanisms are worth studying both theoretically and experimentally.

In particular, they open the possibility of producing multi-antibaryon and multi-antihyperon clusters containing three and more antiparticles. The conventional coalescence model predicts the probabilities to produce these objects which are much smaller as compared to the collective mechanisms [5]. The reason is that the antibaryon clusters are already preformed in normal nuclei due to the additive action of strong scalar and vector fields. Therefore, the fast dynamic process may simply "kick out" these clusters into the upper continuum states. Our present calculations show that the produced antibaryons are relatively close in the momentum space. So they can easily coalesce and form clusters.

Above we focused on the baryon-antibaryon pair production only. But it is clear that the same mechanism can produce also mesons. For instance, the real ω mesons can be generated in the bremsstrahlung process when the four-momenta of quanta satisfy the mass shell constraint $p^2 = m_\omega^2$. The ω meson fusion may result in the two-meson final states ($\pi\pi$, $K\bar{K}$, ...). These channels are characterized by lower threshold and, therefore, by smaller momentum transfers. Since the corresponding coupling constants are also large, one can expect high multiplicities of mesons coherently produced in ultrarelativistic nuclear collisions.

Our last comment is about a possible formulation of the problem on a more fundamental level, introducing quarks instead of baryons. The photon bremsstrahlung radiation from a thermalized quark-gluon plasma was considered in Refs. [41,42]. In the spirit of our approach one can use the effective quark-meson Lagrangians like the linear σ model or the Nambu–Jona-Lasinio model. Then the quark-antiquark production can be studied in time-dependent classical meson fields. This problem was partially addressed in Ref. [43]. The transition on the QCD level, including gluons, is less straightforward. Indeed, the average gluon field in the nucleus vanishes and one should develop a new formalism for considering the pair production by fluctuating fields. The photon-gluon processes leading to the production of the $q\bar{q}$ pairs were studied in Ref. [44].

APPENDIX A: THE DISTRIBUTION OF BREMSSTRAHLUNG PAIRS IN TOTAL MOMENTUM

Below we derive the formula (43) for the distribution of pairs in their total momentum P. Let $f(P,Q)$ to denote the r.h.s. of Eq. (36). Then the total number of $N\overline{N}$ pairs, produced by the bremsstrahlung mechanism, may be expressed as

$$
\begin{aligned}
N_{\text{pair}}^{(1)} &= \int \frac{d^3p_+}{E_+} \int \frac{d^3p_-}{E_-} f(P,Q) \\
&= 4 \int d^4p_+ \int d^4p_- \Theta(p_+^0)\delta(p_+^2 - m_N^2)\Theta(p_-^0) \\
&\quad \times \delta(p_-^2 - m_N^2)f(P,Q).
\end{aligned}
\tag{A1}
$$

Let us make transition to the new variables (37) and (38) and introduce the longitudinal ($Q_\parallel$) and transversal ($\boldsymbol{Q}_\perp$) components of the vector $\boldsymbol{Q}$ with respect to $\boldsymbol{P}$. At given P and $\boldsymbol{Q}_\perp$ the on-mass-shell constraints in Eq. (A1) fix the components $Q_0, Q_\parallel$ of the four-vector Q:

$$
\frac{Q_0}{|\boldsymbol{P}|} = \frac{Q_\parallel}{P_0} = \pm \sqrt{\frac{1}{4} - \frac{m_\perp^2}{M^2}},
\tag{A2}
$$

where $m_\perp^2 \equiv m_N^2 + Q_\perp^2$ and $M^2 = P_0^2 - \boldsymbol{P}^2$.
From Eq. (A1) we get

$$
N_{\text{pair}}^{(1)} = 2 \int d^4P \int d^2Q_\perp \frac{\Theta(P_0)\Theta(M^2 - 4m_\perp^2)}{M\sqrt{M^2 - 4m_\perp^2}} \sum f(P,Q).
\tag{A3}
$$

Here the sum is taken over the two values of $Q_0(Q_\parallel)$ defined in Eq. (A2). A straightforward calculation shows that

$$
\sum f(P,Q) = \frac{d_\tau}{(2\pi)^6}\{(M^2 - 4m_N^2)|S|^2 - M^2 V_\mu^* V^\mu
$$
$$
+ (M^2 - 4m_\perp^2)(V_\mu^* V^\mu + |V_\perp|^2) - 4|\boldsymbol{Q}_\perp V_\perp|^2
$$
$$
+ 8m_N \operatorname{Re}(S^* \boldsymbol{Q}_\perp V_\perp)\}.
\tag{A4}
$$

In Eq. (A4) we took into account the transversality condition, Eq. (21), and denoted by $V_\perp$ the component of V, transversal to $\boldsymbol{P}$.

It can be shown from Eqs. (17) and (40) that the four-vector V^μ is spacelike: $V_\mu^* V^\mu = -|V_\mu^* V^\mu| < 0$. Using Eqs. (95) and (96) one gets

$$
\frac{d^4N^{(1)}}{d^4P} = \frac{2d_\tau}{(2\pi)^6}\int d^2Q_\perp \frac{\Theta(M^2 - 4m_\perp^2)}{M\sqrt{M^2 - 4m_\perp^2}}
$$
$$
\times \{(M^2 - 4m_N^2)|S|^2 + 4m_\perp^2|V_\mu^* V^\mu|
$$
$$
+ (M^2 - 4m_\perp^2)|V_\perp|^2 - 4|\boldsymbol{Q}_\perp V_\perp|^2\}.
\tag{A5}
$$

After calculating the integral in the r.h.s. we arrive at the final result (43).

APPENDIX B: METHOD OF EQUIVALENT MESONS FOR CALCULATING SECOND ORDER EFFECTS IN PAIR PRODUCTION

Below we briefly describe the procedure for calculating the second order contribution to the $N\overline{N}$-pair production. The gauge transformation (66) which simplifies the calculations (see Sec. III) may be obtained after replacing $U_\mu^{(\alpha)}$ in Eq. (61) by

$$
\overline{U}_\mu^{(\alpha)} = U_\mu^{(\alpha)} - \frac{\gamma_0}{\omega_j} k_{j\mu},
\tag{B1}
$$

where $j = 1$ and 2 for $\alpha = p$ and t, respectively. By using Eqs. (67)–(68), in the lowest order in γ_0^{-1} we get

$$
\overline{U}_\mu^{(\alpha)} \approx \left(0, \frac{\gamma_0}{\omega_j}k_{j\perp}, 0\right).
\tag{B2}
$$

From Eqs. (29) and (64), performing the gauge transformation one has

$$
E_+ E_- \frac{d^6N^{(2)}}{d^3p_+ d^3p_-} = \frac{1}{(2\pi)^2} \int \int \frac{d^2k_{1\perp}d^2k_{2\perp}}{(2\pi)^4} g(k_1^2)g(k_2^2)\delta(\boldsymbol{k}_{1\perp} + \boldsymbol{k}_{2\perp} - \boldsymbol{P}_T)
$$

$$
\times \int \int \frac{d^2\tilde{k}_{1\perp}d^2\tilde{k}_{2\perp}}{(2\pi)^4} g(\tilde{k}_1^2)g(\tilde{k}_2^2)\delta(\tilde{\boldsymbol{k}}_{1\perp} + \tilde{\boldsymbol{k}}_{2\perp} - \boldsymbol{P}_T)\frac{k_1^i k_2^l \tilde{k}_1^m \tilde{k}_2^n}{4\omega_1^2\omega_2^2} J_{ilnm},
\tag{B3}
$$

where

$$g(k^2) = AF(\sqrt{-k^2})D_V(k) \qquad (B4)$$

and

$$J_{\mu\nu\mu'\nu'} = \frac{d_\tau}{4} \mathrm{Sp}\{(\hat{p}_- - m_N)H_{\mu\nu}(k_1, p_+, p_-)$$

$$\times (\hat{p}_+ + m_N)H_{\mu'\nu'}(\tilde{k}_1, p_+, p_-)\}. \qquad (B5)$$

The summation in Eq. (B3) goes over the transverse indices $i, l, m, n = 1, 2$ and $\tilde{k}_j$ are obtained from k_j by replacing $k_{j\perp} \rightarrow \tilde{k}_{j\perp}$.

Making the integration over the pair transverse momentum P_T and disregarding the dependence of J_{ilmn} on $k_{1\perp}$ and $\tilde{k}_{1\perp}$, we get

$$\frac{dN^{(2)}}{dy_+ dy_- d^2 Q_T}$$

$$= \frac{\omega_1 \omega_2}{\pi} \frac{dN^{(2)}}{d\omega_1 d\omega_2 dt}$$

$$= \frac{\omega_1 \omega_2}{\pi} \int d^2 r_\perp n(\omega_1, r_\perp) n(\omega_2, r_\perp) \Gamma(\omega_1, \omega_2, t). \qquad (B6)$$

Here

$$n(\omega, r_\perp) = \frac{1}{\pi \omega g_V^2} \left| \int \frac{d^2 k_\perp}{(2\pi)^2} k_\perp e^{ik_\perp r_\perp} g(k^2) \right|^2 \qquad (B7)$$

and

$$\Gamma(\omega_1, \omega_2, t) = \frac{g_V^4}{64\pi\omega_1^2\omega_2^2} \cdot \frac{1}{8}(J_{illi} + J_{ilil} + J_{iill}), \qquad (B8)$$

where the summation over double indices is implied. The calculation of traces in Eq. (B5) shows that the function $\Gamma(\omega_1, \omega_2, t)$ coincides with the cross section $d\sigma/dt$ determined by Eq. (74).

In the case of $\omega\omega$ collisions the characteristic four-momenta squared k^2 entering the arguments of g functions in Eq. (101) are small ($|k^2| \lesssim R^{-2}$) as compared to the cutoff parameter Λ_V^2 in the intrinsic nucleon form factor $f_V(k)$. Substituting $f_V(k) = 1$ into the function $D_V(k)$ [see Eq. (19)] we obtain the expression for the equivalent meson spectrum given by Eq. (75). Finally, we arrive at formula (71) of the main text.

[1] I.N. Mishustin, V.N. Russkikh, and L.M. Satarov, Nucl. Phys. A494, 595 (1989); Yad. Fiz. 54, 260 (1991).

[2] B.D. Serot and J.D. Walecka, Adv. Nucl. Phys. 16, 1 (1985).

[3] J. Schwinger, Phys. Rev. 82, 664 (1951).

[4] I.N. Mishustin, Yad. Fiz. 52, 1135 (1990).

[5] I.N. Mishustin, L.M. Satarov, J. Schaffner, H. Stöcker, and W. Greiner, J. Phys. G 19, 1303 (1993)

[6] J. Schaffner, I.N. Mishustin, L.M. Satarov, H. Stöcker, and W. Greiner, Z. Phys. A 341, 47 (1991).

[7] C.A. Bertulani and G. Baur, Phys. Rep. 163, 299 (1988).

[8] C. Bottcher and M.R. Strayer, Phys. Rev. D 39, 1330 (1989).

[9] G. Baur and N. Baron, Nucl. Phys. A561, 628 (1993).

[10] T. Lippert, U. Becker, N. Grün, W. Scheid, and G. Soff, Phys. Lett. B 207, 366 (1988).

[11] T. Lippert, J. Thiel, N. Grün, and W. Scheid, Int. J. Mod. Phys. A 6, 5249 (1991).

[12] M. Vidović, M. Greiner, C. Best, and G. Soff, Phys. Rev. C 47, 2308 (1993).

[13] J.D. Jackson, Classical Electrodynamics (Wiley, New York, 1975).

[14] D. Vasak, H. Stöcker, B. Müller, and W. Greiner, Phys. Lett. 93B, 243 (1980); D. Vasak, B. Müller, and W. Greiner, Phys. Scr. 22, 25 (1980).

[15] D. Vasak, B. Müller, and W. Greiner, J. Phys. G 11, 1309 (1985); T. Stahl, M. Uhlig, B. Müller, W. Greiner, and D. Vasak, Z. Phys. A 327, 311 (1987).

[16] K.-H. Müller, Nucl. Phys. A372, 459 (1981).

[17] R.Y. Cusson, P.G. Reinhard, J.J. Molitoris, H. Stöcker, M.R. Strayer, and W. Greiner, Phys. Rev. Lett. 55, 2786 (1985).

[18] J.J. Bai, R.Y. Cusson, J. Wu, P.G. Reinhard, H. Stöcker, W. Greiner, and M.R. Strayer, Z. Phys. A 326, 269 (1987).

[19] Chr. Jung, W. Cassing, and U. Mosel, Nucl. Phys. A549, 577 (1992).

[20] Yu.B. Ivanov, Nucl. Phys. A495, 633 (1989).

[21] J.D. Bjorken and S.D. Drell, Relativistic Quantum Mechanics (McGraw-Hill, New York, 1964).

[22] R.A. Williams, S. Krewald, and K. Linen, Phys. Rev. C 51, 566 (1994).

[23] H.C. Dönges, M. Schäfer, and U. Mosel, Phys. Rev. C 51, 950 (1994).

[24] J.J. Sakurai, Currents and Mesons (University of Chicago Press, Chicago, 1969).

[25] L.D. Landau and E.M. Lifshitz, Statistical Physics, Part I (Pergamon, Oxford, 1980).

[26] L.P. Csernai and J.I. Kapusta, Phys. Rev. D 31, 2795 (1985).

[27] U. Katscher, J.A. Maruhn, and W. Greiner, Report No. UFTP-378/1994, University of Frankfurt/M, 1994.

[28] Th. Schönfeld, H. Sorge, H. Stöcker, and W. Greiner, Mod. Phys. Lett. A 8, 2631 (1993).

[29] J.I. Kapusta, Phys. Rev. C 15, 1580 (1977).

[30] C. Bertulani, L. Mornas, and U. Ornik, Report No. GSI-94-89, hep-ph/9412303, 1994.

[31] V.B. Berestetski, E.M. Lifshitz, and L.P. Pitaevski, Relativistic Quantum Theory, Vol. IV (Pergamon, Oxford, 1971).

[32] I.N. Mishustin, L.M. Satarov, J. Maruhn, H. Stöcker, and W. Greiner, Phys. Lett. B 276, 403 (1992).

[33] C.Q. Li, C.M. Ko, X.S. Fang, and Y.M. Zheng, Phys. Rev. C 49, 1139 (1994).

[34] A.M. Rossi et al., Nucl. Phys. B84, 269 (1975).

[35] N.S. Amelin, M.A. Braun, and C. Pajares, Heavy Ion Physics at the AGS, MIT, Cambridge, Report No. MITLNS-2158, 1993, p. 249; N.S. Amelin (private communication).

[36] C.J. Horowitz and B.D. Serot, Nucl. Phys. A368, 303 (1981).

[37] R. Machleidt, Adv. Nucl. Phys. 19, 189 (1989).

[38] M. Rufa, H. Stöcker, J.A. Maruhn, P.-G. Reinhardt, and W. Greiner, J. Phys. G **13**, 143 (1987).

[39] NA35 Collaboration, J. Bächler *et al.*, Phys. Rev. Lett. **72**, 1419 (1994).

[40] A. Jahns, C. Spieles, H. Sorge, H. Stöcker, and W. Greiner, Phys. Rev. Lett. **72**, 3464 (1994).

[41] V.G. Nosov, Zh. Eksp. Teor. Fiz. **96**, 1161 (1989).

[42] J. Kapusta, P. Lichard, and D. Seibert, Phys. Rev. D **44**, 2774 (1991).

[43] C. Greiner, Z. Phys. A **351**, 317 (1995).

[44] M. Greiner, M. Vidović, C. Hoffmann, A. Schäfer, and G. Soff, Phys. Rev. C **51**, 911 (1995).